Solar Modulation Corrections for Cosmic-ray Soil and Snow Sensors Using the Global Neutron Monitor Network

D. L. McJannet[1], and D. Desilets[2]

[1]CSIRO Land and Water, EcoSciences Precinct, Dutton Park, QLD, Australia

[2]Hydroinnova LLC, Albuquerque, New Mexico, USA

Corresponding author: David McJannet (david.mcjannet@csiro.au)

Key Points:

- A new approach for correcting cosmic ray neutron sensor data for the effects of solar activity is presented
- The approach is based on analysis of data from 110 neutron monitor stations from around the world with data spanning more than seven decades
- The approach can be applied at any location on Earth and includes the ability to utilise any neutron monitor as a reference station.

Abstract

Cosmic-ray neutron sensors (CRNS) have been used in many studies for measuring soil moisture and snow pack over intermediate scales. Corrections for geomagnetic latitude, barometric pressure and atmospheric humidity are well established, however, corrections for the effect of solar activity on neutron count rates have been overly simplistic, typically relying on one neutron monitor station and accounting for latitude and elevation crudely or not at all. Recognizing the lack of a generalised and scientifically robust approach to neutron intensity correction, we developed a new approach for correcting CRNS count rates based on analysis of data from 110 quality-controlled neutron monitor stations from around the world spanning more than seven decades. Count rates from each monitor were plotted against the count rates from Climax, CO, USA or Jungfraujoch, Switzerland depending on the time period covered. Relationships between relative counting rates at the site of interest versus the reference neutron monitors were found to be strongly linear. The dimensionless slope of this linear relation, referred to as τ, was shown to increase with increasing geomagnetic latitude and elevation. This dependence of τ on geomagnetic latitude and elevation was represented using an empirical relationship based on a single reference neutron monitor. This generalised approach enables τ to be derived for any location on Earth and also lends itself to roving CRNS studies. The correction procedure also includes a location-dependent normalisation factor which enables easy substitution of an alternative reference neutron monitor into the correction procedure.

Plain Language Summary

Cosmic-ray neutron sensors (CRNS) are used for measuring soil moisture and snow pack at the scale of hectares. Corrections to account for changes in atmospheric pressure and humidity on CRNS measurements are well established and widely applied, however, corrections for changes in incoming cosmic-ray neutron intensity because of solar activity have been overly simplistic. We developed a new approach for correcting CRNS count rates based on analysis of data from 110 neutron monitor stations from around the world with datasets spanning more than seven decades. A strong relationship was found between the relative count rate of neutron monitors from around the world, with the magnitude of the solar correction increasing toward the poles and with elevation. The relationship we found can be applied at any CRNS location based on its elevation, latitude, and longitude to correct for changes to incoming cosmic-ray neutron intensity.

Keywords

Solar modulation correction, neutron monitor, cosmic-ray soil moisture

1 Introduction

Cosmic-ray neutron sensors (CRNS) are now well into their second decade of use for measuring soil moisture and snow pack over intermediate scales (e.g. Baroni et al., 2018; Franz et al., 2012; McJannet et al., 2014; Wallbank et al., 2021; Zreda et al., 2008). These sensors utilise variations in near-surface neutron intensity to detect changes in the hydrologic variable of interest. Application of the technique has occurred through both static (e.g. Bogena et al., 2013;

Desilets et al., 2010; Franz et al., 2012) and mobile sensors (e.g. Desilets et al., 2010; Fersch et al., 2018; Franz et al., 2015; McJannet et al., 2017; Schrön et al., 2021). The basis of the technique is that any deviations from baseline neutron counting rate are proportional to the amount of soil moisture and/or snow water equivalent near the surface. However, several other environmental variables can influence baseline neutron intensity and cause unwanted fluctuations in the raw counting rate, N. These unwanted fluctuations are eliminated by applying correction factors which result in a corrected counting rate, N_{corr}.

The corrected counting rate is calculated by multiplying by a correction factor:

$$N_{corr} = N \cdot F(t) \ . \tag{1}$$

The correction factor $F(t)$ is the product of several individual correction factors (f_i), each of which represent a different process that will influence counting rate:

$$F(t) = \prod f_i, \tag{2}$$

The individual f_i include; f_{bar} which corrects for the for effect of barometric pressure variations which can have a significant influence on N (see Zreda et al. (2012)), f_{hum} which corrects for the effects of atmospheric humidity on N (see Rosolem et al. (2013)), and f_{lat} which normalises for geomagnetic latitude effects during mobile surveys (see Dorman et al. (2000)). For this work we concentrate on quantifying f_{sol}, which is related to solar activity.

f_{sol} accounts for changes in the flux of primary cosmic ray neutrons that reach the Earth's atmosphere after passing through the magnetosphere. This primary flux, and (indirectly) the flux of secondary neutrons at Earth's surface are influenced by the solar wind and its interactions with the magnetosphere. When the sun is active, solar magnetic fields are stronger

and primary intensity is reduced. Naturally, the opposite happens when the sun is quiet. This work is concerned with the influence of solar activity on secondary neutrons at ground level.

The fluxes of fast and slow neutrons at ground level ultimately depend on the fluxes of high-energy secondary neutrons. High energy neutron fluxes are measured by devices known as neutron monitors (Flückiger & Bütikofer, 2009; Mavromichalaki et al., 2011; Simpson, 2000; Väisänen et al., 2021). Beginning with the International Geophysical Year (IGY; 1957-58) project and continuing on with the International Quiet Sun Year (IQSY; 1964-65) numerous neutron monitors were installed around the world. Although most of the original IGY and IQSY monitors are now defunct, it is possible to use those archived data together with data from surviving and more recently added sites to correct CRNS data. An example of the long-term variation in neutron monitor count rate in response to solar activity is shown in Figure 1 for the Climax Neutron monitor in Colorado, USA - one of the first and longest running stations in the world. In this figure the dashed blue line represents the long-term average count rate. Variations in neutron intensity of ±10% (shaded area) are commonly observed. Clearly, it is essential to correct CRNS count rates to account for this variation in incoming neutron flux, which is presumably of a similar magnitude for the CRNS.

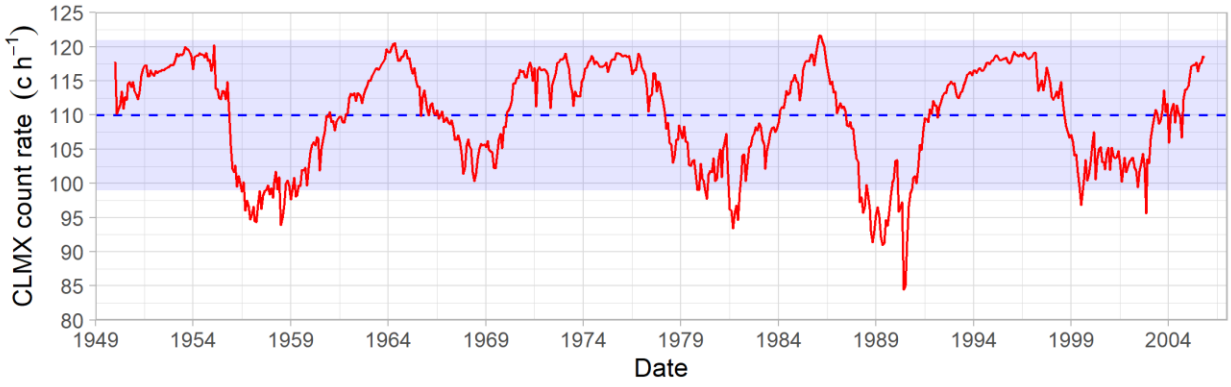

Figure 1. Long-term variation is neutron counting rate at Climax, CO, USA. The blue line indicates the mean counting rate and the blue shaded area represents the mean ±10%. Average monthly values expressed as hourly counting rate are presented (source: **www.nmdb.eu**).

The effect of solar activity on CRNS count rates can be removed using the following formula:

$$f_{sol} = \frac{N_r}{N}, \tag{3}$$

where N is the neutron monitor count rate at the time of interest and N_r is a reference counting rate for a given neutron monitor which is often specified as a count rate at a specific point in time or averaged over a set time interval. We note that in other studies f_{sol} is given as the inverse of Equation 3 (e.g. Zreda et al. (2012)), in such cases the CRNS count rate is divided by this correction factor. The form we present here makes all correction factors multiplicative. A challenge is that f_{sol} at any given the location on Earth depends (mainly) on elevation and latitude (or more precisely, atmospheric shielding depth (x) and cutoff rigidity (R_c)).

As a first approximation, the US based COSMOS network (Zreda et al., 2012), and COSMOS-UK (Evans et al., 2016), both located at relatively high geomagnetic latitudes, simply use a correction based on a single neutron monitor at Jungfraujoch (JUNG) in Switzerland

(Flückiger & Bütikofer, 2009), but other networks have introduced different approaches to account for the regional differences in cutoff rigidity. Some investigators have been fortunate enough to have a neutron monitor close by, e.g. Jitnikovitch et al. (2021) were able to use the Inuvik Neutron monitor while working near Inuvik, NT, Canada; Howat et al. (2018) were able to use the Thule Neutron Monitor while working in the Greenland Ice Sheet; and for Gugerli et al. (2022) the Jungfraujoch monitor was ideally located. In these rare cases the user can directly utilize nearby data. But most do not have this option. Ideal or not, direct use of Jungfraujoch data has become a common fallback option. The Australian CosmOz network (Hawdon et al., 2014) experiences a large range in cut-off rigidity with values of 14.4 GV in the north through to 1.76 GV in the south and is more than 14,000 km from Jungfraujoch. To address this issue the CosmOz network applies an intensity correction using Equation 3 but utilises neutron monitors with R_c as close as possible to the R_c of a given CRNS site. The COSMOS-Europe network (Bogena et al., 2022) has implemented the intensity correction factor described by Hawdon et al. (2014) and Schrön et al. (2015):

$$f_{sol} = \left[1 + s\left(\frac{N}{N_r} - 1\right)\right]^{-1} \tag{4}$$

where s is an amplitude scaling factor used to adjust for geomagnetic effects:

$$s = 1 - 0.075\left(R_c - R_{c\_ref}\right), \tag{5}$$

where R_c is the effective cutoff rigidity for the CRNS site and R_{c_ref} is the effective cutoff rigidity for the reference neutron monitor. The underlying derivation of this relationship has not been published in the literature and it is considered a working model based on preliminary analysis of neutron monitors spanning a large range in R_c which was undertaken by COSMOS network affiliates. The correction itself is of a linear form.

Recognizing the lack of a generalised and scientifically robust approach to neutron intensity correction, this paper proposes a new approach for correcting CRNS count rates based on analysis of data from many of the 146 neutron monitors that have ever existed, which provide coverage a from the high arctic/south pole to the equator and from sea level to 5200 meters. The correction procedure utilises a reference neutron monitor and scales the temporal variation at the reference monitor to the cutoff rigidity and atmospheric depth of a different site.

The approach developed in this study addresses variations in the cosmic-ray baseline as observed by ground level instruments on Earth. These changes are due mainly to variations in the strength of the interplanetary magnetic field, and the ability of that field to deflect primary cosmic rays away from Earth. From a phenomenological perspective the level of this baseline corresponds to the heliospheric modulation strength as represented, for example, by the force field approximation and its associated modulation parameter (Gleeson & Axford, 1968). In terms of solar processes, this corresponds to changes in the background coronal source flux that is carried by the solar wind (Lockwood et al., 1999). Most importantly, the entire Earth is impacted by the processes we seek to capture here, and in a way that is more or less predictable based on the atmospheric depth and cutoff rigidity.

Our method does not account for violent eruptive solar events i.e., coronal mass ejections and solar flares that perturb the heliosphere and can send anomalous magnetic fields hurtling toward Earth. In terms of terrestrial cosmic ray intensity, such events are closely associated with perturbations of ground level neutron intensity, including Forbush decreases and ground level enhancements. From our point of view, these phenomena share three important characteristics: they tend to be (1) transitory on the scale of hours to days; (2) anisotropic in how they impact earth; (3) and relatively uncommon (counted in events per year), at least for the larger events.

These types of events, which originate from specific regions on the sun, and impact specific regions of Earth (and in different ways from event to event) will require more complex corrections, including more sophisticated models and inclusion of additional types of heliospheric observation.

2 Materials and Methods

2.1 Site Selection and Data Processing

We utilised both the Neutron Monitor Database (NMDB; www.NMDB.eu) and the World Data Centre for Cosmic Rays (WDC-CR; https://cidas.isee.nagoya-u.ac.jp/WDCCR/). Both offer open access to a large catalogue of neutron monitor data. Some monitors deliver data through both databases. WDC-CR holds a large amount of data from monitors that have long-ceased operation. Data from all available stations from NMDB were downloaded and then any extra stations available from WDC-CR were also added to the total pool used for analysis.

We performed several data quality controls. Neutron monitor data are often collected at high temporal resolution, however in this study we collated monthly average neutron count rates. Monthly count rates are considered acceptable as the primary goal is to correct longer-term fluctuations in neutron intensity. Other methods will be required to accurately correct for anomalous short term variations (e.g., Forbush events (Mishra et al., 2005)), as these tend to impact the Earth unevenly and in different ways from event to event. The effect of utilizing hourly, daily or monthly count rates in the analysis will be further explored in the Results section.

As the first requirement only neutron monitors with at least 24 months of data were included in analysis. Neutron monitor datasets with less than 24 months of data were excluded as these sites introduced excessive uncertainty in later analysis. This uncertainty was typically the result of limited temporal variation in neutron counts. For a month's data to be included in the analysis the month also needed to be more than 90% complete. Monthly data were also filtered to exclude unphysical step changes in reported counting rate. Such changes sometimes occur due to modifications to equipment and site conditions; while scaling factors were usually provided to correct for this, the transition between count rates was not always smooth resulting in banding in data which did not reflect realistic changes in count rate. When such conditions occurred the period of data with the longest continuous scaling factor was utilized and all other data was excluded.

The R_c for each neutron monitor was specified by either the NMDB or WDC-CR database. It is also important to consider the effect of differences in atmospheric depth, x (g cm^{-2}), on the neutron monitor variations. For each neutron monitor, x was derived from:

$$x = 10p/g, \quad (6)$$

where p is the reference atmospheric pressure (mb) of the neutron monitor which was calculated using standard formulas based on site elevation (U.S. Standard Atmosphere, 1976) and g is local acceleration due to gravity (m s^{-2}). Procedures for calculating p and g are given in Supporting Information 1.

2.2 Neutron Intensity Solar Correction

The primary aim of this investigation was to derive a neutron intensity correction for solar activity for any CRNS location based on a reference neutron monitor. As such, the reference neutron monitor needed to have long-term and reliable measurements. In this study, two reference neutron monitors were utilised to cover the entire era of neutron monitor operation. The first reference monitor was the Climax station (CLMX) in Colorado, USA, which commenced operation in 1951 and operated until 2006. The second reference monitor was the Jungfraujoch station (JUNG) in Switzerland which commenced operation in 1958 and is still operational today. The JUNG reference monitor was included to extend the data set from 2006 onwards,. The process of scaling the relationships between JUNG and neutron monitors to an equivalent relationship with the CLMX monitor is discussed below.

The relationship between each neutron monitor and its given reference neutron monitor (CLMX or JUNG depending on the time period) was assessed using normalised counting rates. For any given neutron monitor, monthly count rates (N) were normalised by dividing by the average count rate (N_r) for all available months. The corresponding reference neutron monitor count rates (N^{ref}) were normalised using the average count rate (N_r^{ref}) from matching months.

Analysis was undertaken using the following equation:

$$\frac{N}{N_r} = \tau \frac{N^{ref}}{N_r^{ref}} + 1 - \tau, \tag{7}$$

which has the linear form, $y = mx + b$, where the slope (m) corresponds to τ and the intercept $b = 1 - \tau$. The value τ is the dimensionless slope of the linear regression between the site of interest and the reference site. The derivation of Equation 7 is given in Supporting Information 2.

222 Based on Equation 7, the value of τ has been calculated for the 110 neutron monitor data
223 sets collated for this study. These τ values will then be used along with the corresponding R_c and
224 x values for each site to build an empirical relationship to enable τ to be predicted for any CRNS
225 location.

226 As mentioned above, most τ values were determined between the monitor of interest and
227 CLMX, however the τ for some monitors, particularly newer ones, had to be determined between
228 the site of interest and JUNG. To standardise all τ values to CLMX as the reference site, the τ
229 values derived with JUNG as a reference site were divided by 1.29 which is the τ value for
230 CLMX versus JUNG (data below), indicating a ~30% greater sensitivity for CLMX.

231

232 **3 Results and Discussion**

233 3.1 Site Selection and Data Processing

234 After filtering, a final set of 110 neutron monitors was extracted from the NDMB and
235 WDC-CR databases. This consisted of 67 datasets from WDC-CR and 43 from NMDB (Figure
236 2). These sites cover a large range of R_c from a minimum of 0.0 GV to a maximum of 16.8 GV.
237 There is a distinct decline in neutron monitor numbers with increasing R_c reflecting the focus of
238 neutron monitoring efforts in high latitude locations (Figure 3). The site details for each of the
239 neutron monitors utilised and the reference site against which they are compared (CLMX or
240 JUNG) are given in Appendix A (Table A1). In total, 95 neutron monitors used CLMX as the
241 reference monitor and 15 used JUNG as the reference monitor.

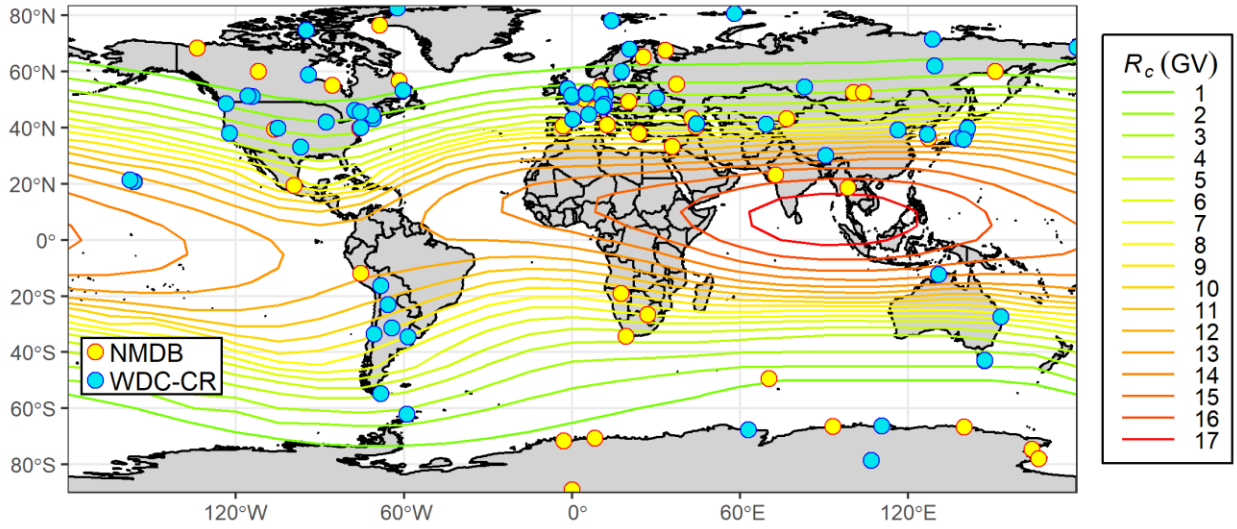

242

243 **Figure 2.** Location of neutron monitor stations utilized in this study. The yellow points indicate
244 stations from NMDB while the blue points show stations from WDC-CR. Effective vertical
245 cutoff rigidities for the epoch 2020 are also overlaid on the map (source: Gerontidou et al.
246 (2021)).

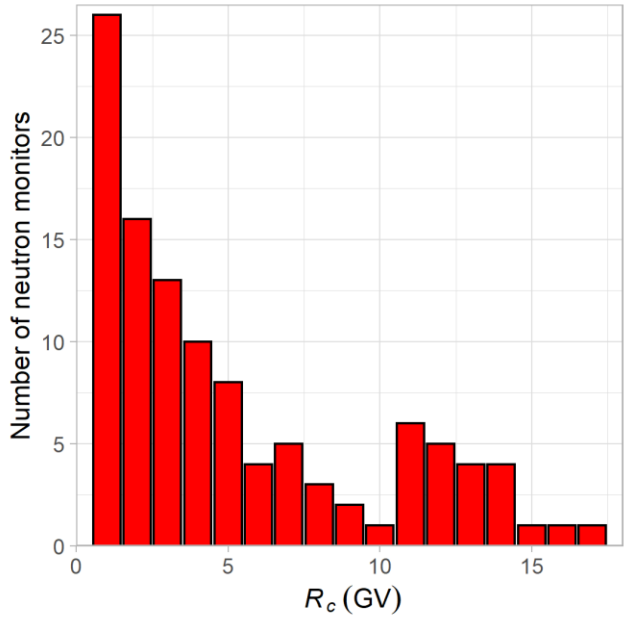

247

248 **Figure 3.** Histogram of the number of neutron monitors in each 1 GV range of R_c.

Figure 4 shows a comparison of neutron monitor data from Kerguelen Islands (KERG) and Potchefstroom, South Africa (PTFM) against the CLMX reference dataset for a 5-year period between 1995 and 2000 with data presented at hourly, daily and monthly timescales. Count rates for all time intervals were normalised to the average of the dataset. These example datasets suggest that the selection of timescale has minimal impact on the derived τ values (Equation 7) for these sites.

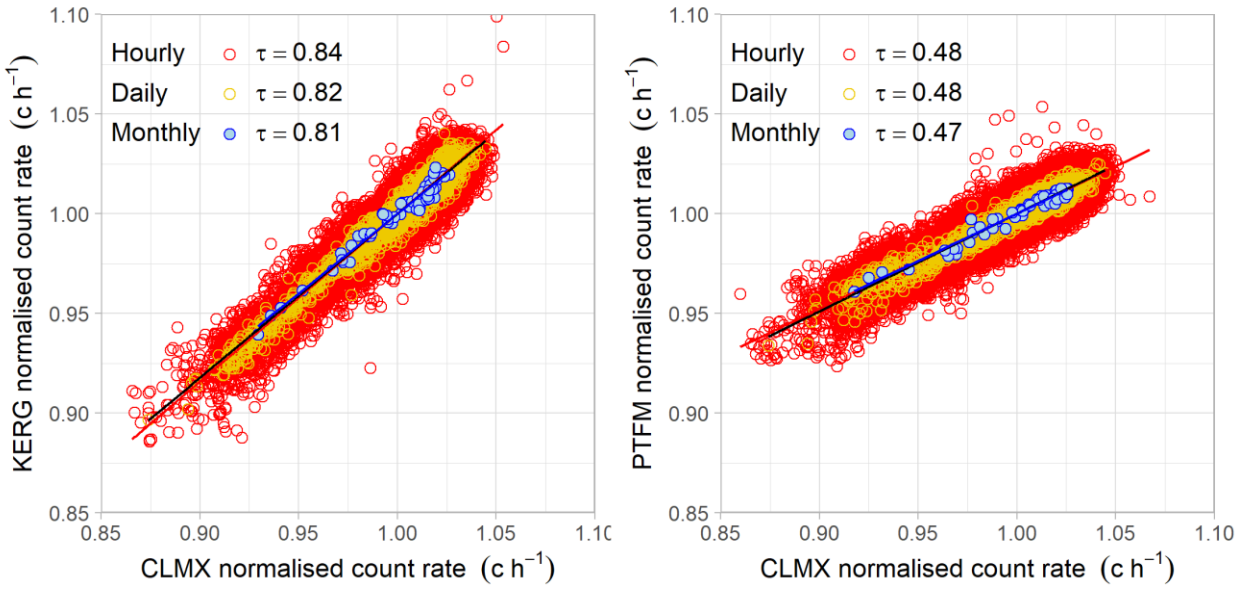

Figure 4. Correlation between KERG (R_c=1.14 GV, x=1028.8 g cm^{-2}) and PTFM (R_c=6.98 GV, x=880.0 g cm^{-2}) sites using hourly, daily, and monthly data showing the minimal effect of utilizing monthly averages. The fitted lines, Equation 7, for hourly, daily, and monthly data are colored red, black and blue, respectively.

3.2 Neutron Intensity Solar Correction

Figure 5 shows the τ relationship with respect to CLMX for specified neutron monitors. These 12 sites are a small sample of the 110 neutron monitors available and have been selected to include at least 48 months of data and show the results across a range of R_c values. Equivalent relationships for all 110 neutron monitors are given in Appendix B. The slope of the relationship, τ, is displayed on each plot in the form of Equation 7 along with the number of months of comparison data (n) and the coefficient of determination (R^2). All relationships are shown to be strongly linear giving confidence in scaling of observations between neutron monitors.

An important behaviour is the reduction in τ with increasing R_c values. This clearly illustrates the suppression in solar intensity corrections at higher R_c (lower geomagnetic latitude). The derived τ values, standard error of the regression line (se), number of monthly observations used (n), and coefficient of determination (R^2) for each of the 110 neutron monitors are given in Appendix A (Table A1). The values of R^2 tended to be lower for sites with smaller datasets and these also tended to be sites with higher R_c. The largest comparison dataset spanned 576 months (Moscow, MOSC) and the smallest was just 24 months (Heiss Island, HEISS).

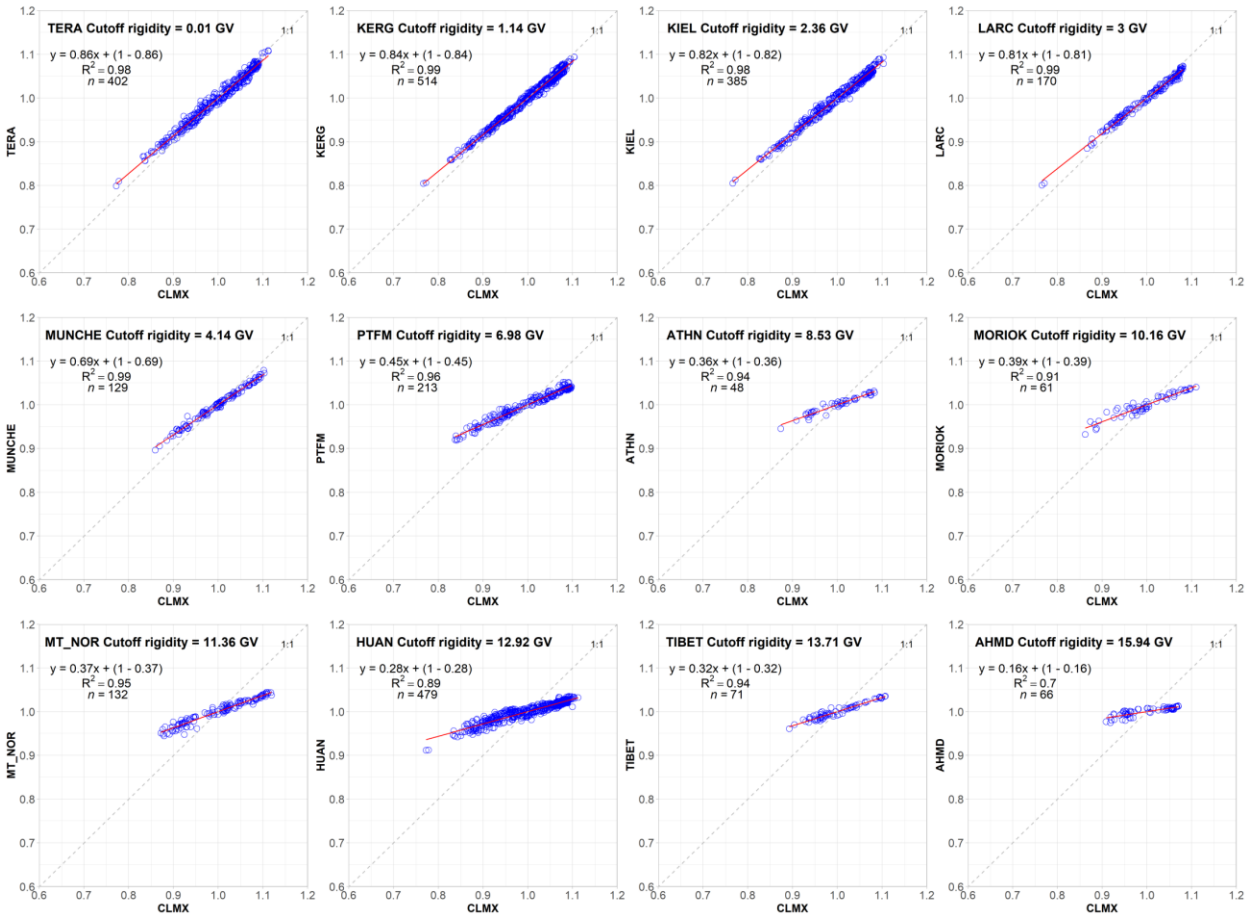

Figure 5. Example data showing the relationship between normalized CLMX neutron counts (reference monitor) and normalized neutron counts from comparison neutron monitors. Cutoff rigidity or comparison monitors increases from left to right and down the figure. Full set of 110 neutron monitor comparisons is given in Appendix B.

Before a generalised correction for neutron flux intensity can be derived it is also necessary to account for the effects of atmospheric depth, x, at each site. The combined effects of both x and R_c on τ are shown in Figure 6. In this figure, τ values for monitors using CLMX as a reference site have been adjusted as outlined in the Methods section.

A best fit prediction surface was derived for the data points using the following empirical relation

$$\tau(x, R_c) = \varepsilon K(c_0 x + c_1)\left[1 - exp\left(-[c_2 x + c_3]{R_c}^{c_4 x + c_5}\right)\right], \quad (8)$$

where K is a location-dependent normalisation factor (discussed below) and ε is a correction factor that adjusts the sensitivity of the standard lead neutron monitor to that of rock, currently assumed to be $\varepsilon = 1$. This equation reduces to a Dorman type function with R_c (Dorman et al., 1970; Dorman et al., 2000) and a linear function with x . Coefficients c_i are provided in Table 1. The standard error of the estimate of this fitted surface was 0.08.

The value of τ is greatest and the variation in neutron intensity correction over time is most enhanced at low R_c and low x (Figure 6). On the other hand, at high R_c and high x, the value of τ is lowest and the variation in neutron intensity correction over time is most supressed. Therefore, CRNS sites corrected using reference neutron monitors at vastly different R_c and x, without inclusion of these effects, will have the highest degree of uncertainty in neutron intensity correction. Even at locations in close proximity to a nearby neutron monitor, or with similar R_c, elevation differences should be considered. Elevation effects are particularly important at R_c < 6 GV. Although the uncertainty in correction will be higher at low R_c, the correction itself will be smaller, so the uncertainty is less important in such cases.

The scaling factor K allows one to use any neutron monitor on Earth as the reference monitor. It relates the sensitivity of the new reference neutron monitor (τ_{NEW}) to the sensitivity at CLMX (τ_{JUNG}). The value of K depends on the x and R_c of the reference neutron monitor that is being used for the correction. Since τ_{CLMX} is defined to be 1 in our analysis, the factor is simply:

$$K = \frac{1}{\tau_{NEW}}. \quad (9)$$

The move to an alternative neutron monitor is a simple two-step process; firstly, Equation 8 is used to calculate τ_{NEW} by specifying the x and R_c as those of the new neutron monitor but setting K = 1.0. Next, τ_{NEW} is used in Equation 9 to determine the K for the alternative neutron monitor. A worked example of application of Equation 8 to an alternative neutron monitor is given in Supporting Information 1.

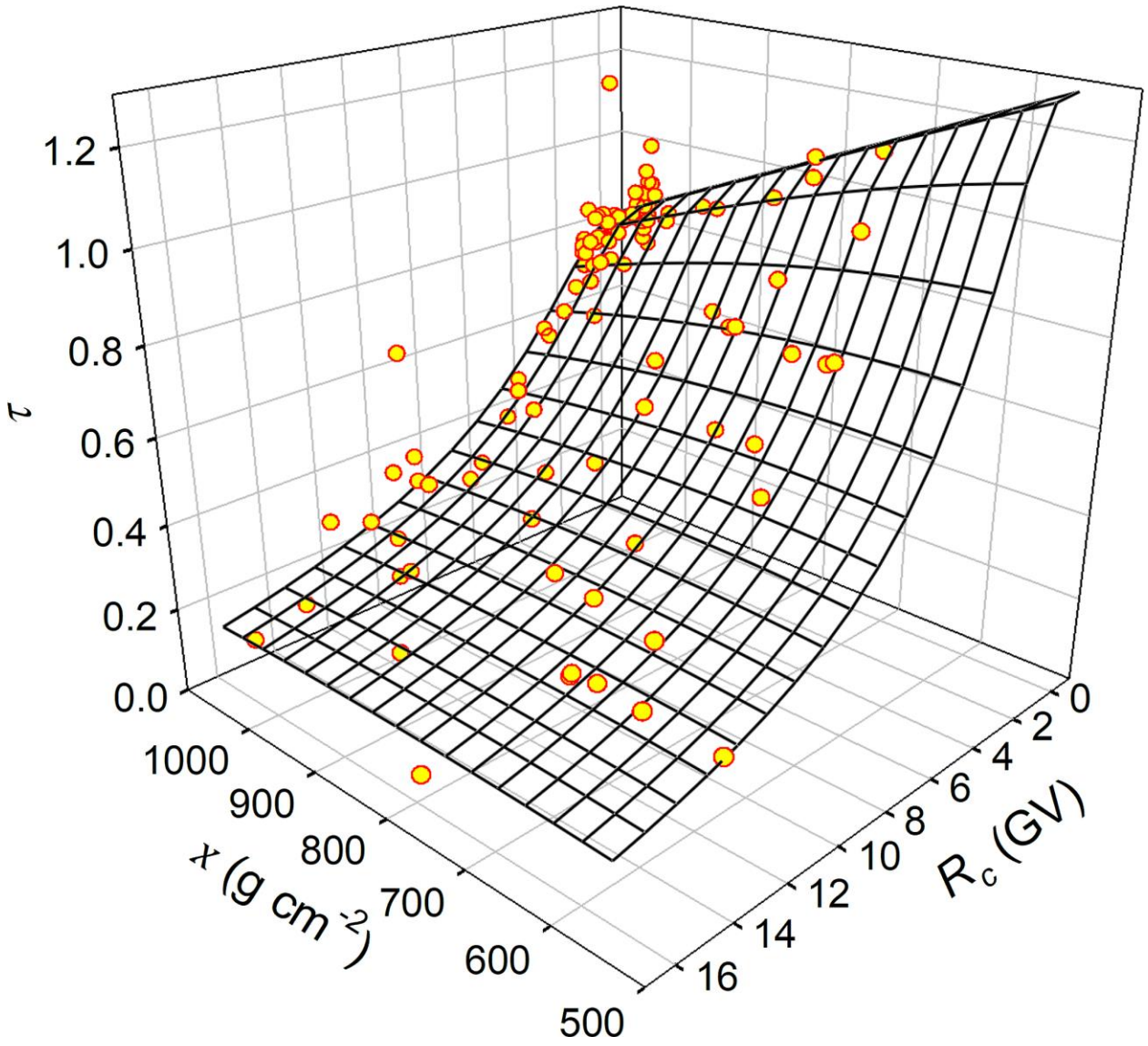

Figure 6. Scatter plot of τ against x and R_c and surface fitted to the data points using Equation 8.

315

316 **Table 1.** Parameters for calculating τ using Equation 8.

Parameter	Value
c_0	-0.0009
c_1	1.7699
c_2	0.0064
c_3	1.8855
c_4	0.000013
c_5	-1.2237

317

318 Using the empirical relationship derived in this study to determine τ from R_c and x, the
319 solar correction, f_{sol}, for CRNS counting rates can be determined by:

$$f_{sol} = \left[\tau \frac{N^{ref}}{N_r^{ref}} + 1 - \tau\right]^{-1}. \quad (10)$$

320

321 **3.2.1 Comparison of neutron intensity correction methods**

322 Three alternative methods have been presented for determining for f_{sol} for a CRNS site,
323 these are:

324 1. Equation 3 which gives the normalised counting rate for the reference neutron monitor (in
325 this work JUNG is the default),

2. Equation 4 which scales the normalised counting rate at the reference monitor to the location of interest (based on R_c), and

3. Equation 10 (formulated in this study) which gives τ as a function of x and R_c.

The relative performance of these three methods is presented in Figure 7 for the DARW (Darwin, Australia) and OULU (Oulu, Finland) neutron monitors. The f_{sol} calculated directly at the selected monitor (either DARW or OULO) as, N_r/N is considered the point of truth for testing the three methods.

The DARW monitor is chosen as it represents a site with very high x and R_c (low elevation and low latitude) it is also in the southern hemisphere, where most historical data are lacking. Direct use of Equation 3 produces an unreliable estimate of f_{sol}; in this case the reference neutron monitor (JUNG) experiences greater solar variations than what would be expected at DARW (see Figure 6) due to its higher latitude and altitude. Equation 4 and Equation 10 both produce f_{sol} estimates typically within ± 1% of the true value. The improved performance of these two approaches reflects the inclusion of the R_c scaling which supresses the effects of solar activity at this low latitude site. While Equation 4 does not include a correction for x, it still performs well as elevation effects are minimal at sites with high R_c (see Figure 6).

The OULU monitor represents a site with low elevation (high x) and high geomagnetic latitude (very low R_c). Surprisingly, Equation 3 performed much better at OULU but closer inspection reveals that this is because the value of τ for JUNG, 0.74, is similar to that derived at OULU, 0.84. This is a fortuitous effect as a result of the interaction of x and R_c on derived τ. The performance of Equation 4 was much reduced at OULU as the effects of x on solar activity are not accounted for. At high geomagnetic latitude, f_{sol} varies strongly with x (see Figure 6).

Another issue with Equation 4 (which we note was only ever a working model) is the linear nature of the correction. Numerous latitudinal surveys of neutron intensity have shown non-linear relationships between R_c and neutron counts (Dorman et al., 1970; Dorman et al., 2000; Heber et al., 2015; Mangeard et al., 2016). With the inclusion of corrections for the effects of x and R_c on f_{sol}, Equation 10 was again the best performer at OULU with the least scatter in observed differences (typically within ± 1% of the true value)

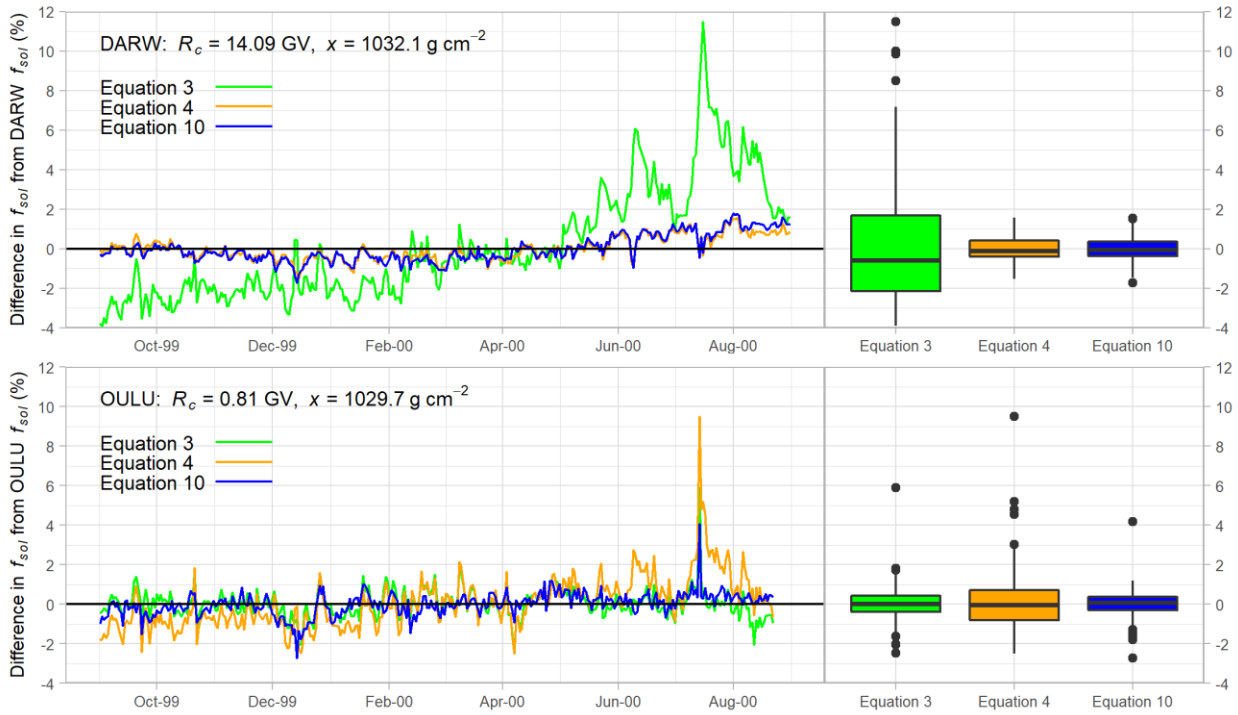

Figure 7. Comparison of the percentage difference in f_{sol} values calculated using Equation 3, Equation 4 and Equation 10 as compared to the values directly calculated at the selected neutron monitor. Box plots to the right of each plot illustrate the accuracy and scatter in results for each equation.

The strength of the new correction we propose is that it requires only one neutron monitor to be used for CRNS corrections and can be applied at any location. An online calculator

for providing hourly neutron intensity corrections at any CRNS station location based on the JUNG neutron monitor data is available at https://crnslab.org/util/solar.php. This calculator uses the average count rate on 1 May 2011 as the reference count rate. A separate calculator for determining R_c is available at https://crnslab.org/util/rigidity.php.

Another key feature of the proposed approach is the ability to switch between neutron monitors and easily use a new station as the reference dataset. Such a capability is useful as neutron monitors cease operation, new neutron monitors come online or when one wishes to use a nearby neutron monitor The approach developed also lends itself to application in roving CRNS studies. In rover surveys where vast distances and varying landscapes can be covered, (e.g., the transregional, train-based CRNS surveys of Schrön et al. (2021)), a spatially varying correction could be applied to account for atmospheric and geomagnetic variations, with the added advantage that the input data required for the new neutron intensity correction (i.e., latitude, longitude and elevations) will already be collected as part of the standard rover measurement procedures.

5 Conclusions

Cosmic-ray neutron sensors (CRNS) have now been used for over two decades to measure soil moisture and snow pack at intermediate scales using both static and roving sensors. Unwanted temporal fluctuations are eliminated by applying correction factors. Corrections for geomagnetic latitude, barometric pressure and atmospheric humidity are well established, however, corrections for the effect of solar activity on neutron count rates have received little attention to date and relatively simple corrections utilising neutron monitor data have been applied across most studies.

Recognizing the lack of a generalised and scientifically robust approach to neutron intensity correction, this study set out to develop a new approach for correcting CRNS count rates based on analysis of data from many neutron monitors located around the world. Neutron monitor data from the Neutron Monitor Database (www.NMDB.eu) and the World Data Centre for Cosmic Rays (https://cidas.isee.nagoya-u.ac.jp/WDCCR/) were utilised. In total, 110 high quality neutron monitor stations, spanning over 70 years of observations, were used in the final dataset and each of these had at least 24 months of data. Each of these neutron monitors was compared to one of two reference neutron monitors which were selected as reliable, long-term stations.

Relationships between counting rates at the site of interest and the reference neutron monitor were found to be strongly linear and the two data sets were shown to be related by a scaling factor referred to as τ. The value of τ was shown to increase with increasing geomagnetic latitude (decreasing R_c). It was also established that elevation influences τ as greater atmospheric depth acts to supresses the influence of solar activity.

In order to develop a generalised correction for neutron intensity, the combined effects of both R_c and x on τ were represented using a 3-dimensional relationship. The derived empirical best-fit equation utilised a single reference neutron monitor and enables τ to be derived for any CRNS location based on its elevation, latitude, and longitude. The scaling factor τ is enhanced at low R_c and low x, and is most supressed at high R_c and high x.

Another feature of the generalised correction for neutron flux intensity is the inclusion of a location-dependent normalisation factor which enables easy substitution of an alternative reference neutron monitor into the correction procedure. The proposed formulation can be easily

adopted at static CRNS stations and lends itself to roving CRNS studies where R_c and x will vary across the survey area.

Acknowledgments

The authors thank the anonymous reviewers for whose comments helped to improve this manuscript. We acknowledge the NMDB database www.nmdb.eu, founded under the European Union's FP7 programme (contract no. 213007) for providing data. We also thank the Institute for Space Earth Environmental Research at Nagoya University for hosting the World Data Center for Cosmic Rays (https://cidas.isee.nagoya-u.ac.jp/WDCCR/). This study would not have been possible without these data sources or the organisations which manage individual neutron monitors. We are grateful to the efforts of these organisations and their provision of open access data. In the interests of brevity, we have listed these organisations in Supporting Information 3. David McJannet received funding for this research through the Terrestrial Ecosystem Research Network (TERN) which is part of the National Collaborative Research Infrastructure Strategy (NCRIS) program.

Supporting Information

Filename	Description
Supporting Information 1 – Example Calculations.xlsx	Document S1
Supporting Information 2 – Derivation of Solar Correction Equation.docx	Document S2
Supporting Information 3 – Neutron Monitor Acknowledgments.docx	Document S3

Appendix A: Site details and derived values for all monitors used in the study

Table A1. Site code, database name, latitude, longitude, elevation, cutoff rigidity (R_c), atmospheric depth (x), number (n) of months data used for relationship derivation, standard error (se) of the prediction, correlation coefficient (R^2), scaling factor (τ), and location-dependent normalisation factor (K) should this neutron monitor be used as a reference site in Equation 8. * indicates τ values using JUNG as a reference site which have been subsequently scaled to CLMX.

Site code	Database name	Lat. (deg)	Lon. (deg)	Elev. (m)	R_c (GV)	x (g cm^{-2})	n (month)	se	R^2	τ	Monitor K
ALERT	WDC-CR	82.50	-62.33	57	0	1023.7	257	0.010	0.97	0.913	1.18
BARENT	WDC-CR	78.06	14.22	51	0	1024.6	35	0.039	0.95	1.004	1.18
RESOLU	WDC-CR	74.69	-94.91	17	0	1028.8	47	0.018	0.98	0.835	1.18
VOSTOK	WDC-CR	-78.47	106.87	3488	0	670.0	60	0.034	0.96	1.321	0.86
TERA	NMDB	-66.65	140.00	32	0.01	1027.5	402	0.006	0.98	0.862	1.18
WILKES	WDC-CR	-66.27	110.53	10	0.01	1030.2	84	0.016	0.97	0.875	1.19
MRNY	NMDB	-66.55	93.02	30	0.03	1027.7	145	0.037	0.88	0.916*	1.18
HEISS	NMDB	80.62	58.05	20	0.1	1028.2	50	0.068	0.81	0.943	1.18
NEU3	NMDB	-70.63	8.26	40	0.1	1026.3	204	0.010	0.98	0.836*	0.90
SOPO	WDC-CR	-90.00	0.00	2820	0.1	729.4	24	0.046	0.95	1.107	1.18
CHURCH	WDC-CR	58.75	-94.08	39	0.21	1027.3	158	0.009	0.98	0.891	1.18
MAWSON	WDC-CR	-67.60	62.88	0	0.22	1031.3	153	0.007	0.99	0.889	1.19
FSMT	NMDB	60.02	-111.93	180	0.3	1010.1	74	0.020	0.96	0.895	1.16
INVK	NMDB	68.36	-133.72	21	0.3	1028.7	83	0.013	0.98	0.822	1.18
JBGO	NMDB	-74.60	164.20	29	0.3	1027.4	67	0.062	0.80	0.783*	1.18
MCMU	NMDB	-77.90	166.60	48	0.3	1024.9	557	0.007	0.96	0.861	1.18
NAIN	NMDB	56.55	-61.68	46	0.3	1026.6	73	0.021	0.96	0.854	1.18
PWNK	NMDB	54.98	-85.44	53	0.3	1025.9	75	0.022	0.95	0.806	1.18
THUL	NMDB	76.50	-68.70	26	0.3	1027.7	360	0.007	0.97	0.838	1.18
CAPE_S	WDC-CR	68.55	180.32	0	0.45	1031.3	143	0.005	0.99	0.867	1.19
TIXIE	WDC-CR	71.36	128.54	0	0.48	1031.1	121	0.010	0.98	0.839	1.19
KIRUNA	WDC-CR	67.83	20.43	400	0.54	983.3	59	0.012	0.99	0.867	1.13
GOOSE	WDC-CR	53.27	-60.40	46	0.64	1026.9	177	0.010	0.98	0.900	1.18
APTY	NMDB	67.57	33.40	181	0.65	1009.4	77	0.008	0.99	0.839	1.16
SNAE	NMDB	-71.67	-2.85	856	0.73	930.6	465	0.010	0.95	0.909	1.07
OULU	NMDB	65.05	25.47	15	0.81	1029.7	512	0.005	0.98	0.839	1.19
CALGAR	WDC-CR	51.08	-114.13	1128	1.08	902.0	218	0.014	0.95	0.922	1.04
SULPHU	WDC-CR	51.20	-115.60	2283	1.09	782.5	122	0.010	0.99	1.088	0.94
DEEP_R	NMDB	46.10	-77.50	145	1.14	1015.6	514	0.004	0.99	0.861	1.19
KERG	WDC-CR	-49.35	70.25	33	1.14	1028.8	424	0.006	0.98	0.837	1.17
SULIGY	WDC-CR	51.20	-115.60	2283	1.14	782.5	83	0.013	0.99	1.044	0.94
OTTAWA	WDC-CR	45.44	-75.68	57	1.22	1026.3	85	0.016	0.97	0.847	1.18
UPPSAL	WDC-CR	59.86	17.62	0	1.43	1031.9	40	0.021	0.98	0.623	1.19

Site code	Database name	Lat. (deg)	Lon. (deg)	Elev. (m)	R_c (GV)	x (g cm^{-2})	n (month)	se	R^2	τ	Monitor K
MT_WAS	WDC-CR	44.27	-71.30	1909	1.46	820.3	370	0.008	0.98	0.988	0.98
DURHAM	WDC-CR	43.10	-70.83	0	1.58	1033.5	202	0.007	0.98	0.807	1.20
YAKUTS	WDC-CR	62.01	129.43	105	1.65	1019.0	328	0.010	0.96	0.860	1.19
CHICAG	WDC-CR	41.83	-87.67	200	1.72	1009.4	66	0.013	0.98	0.749	1.18
MT_WEL	WDC-CR	-42.92	147.25	725	1.8	947.8	143	0.006	0.99	0.884	1.11
KINGST	WDC-CR	-42.99	147.29	65	1.81	1025.5	74	0.012	0.98	0.755	1.20
VICTOR	WDC-CR	48.42	-123.32	71	1.86	1024.3	26	0.047	0.96	1.175	1.20
HOBART	WDC-CR	-42.88	147.33	0	1.88	1033.5	79	0.022	0.95	0.805	1.21
SWARTH	WDC-CR	39.90	-75.35	80	1.92	1024.0	161	0.007	0.99	0.806	1.21
MGDN	NMDB	60.04	151.05	220	2.1	1005.3	335	0.007	0.98	0.834	1.20
LEEDS	WDC-CR	53.80	-1.55	72	2.2	1023.7	171	0.011	0.98	0.873	1.23
KIEL	NMDB	54.34	10.12	54	2.36	1025.8	385	0.005	0.98	0.818	1.25
KIEL2	NMDB	54.34	10.12	54	2.36	1025.8	39	0.028	0.98	0.869*	1.25
NEWK	NMDB	39.68	-75.75	50	2.4	1027.7	508	0.003	0.99	0.806	1.25
MOSC	NMDB	55.47	37.32	200	2.43	1008.1	576	0.008	0.95	0.818	1.23
MCRL	NMDB	55.47	37.32	200	2.46	1008.1	117	0.024	0.95	0.863*	1.24
LONDON	WDC-CR	51.53	-0.10	45	2.73	1027.2	35	0.031	0.96	0.890	1.29
NEDERH	WDC-CR	52.23	5.08	-2	2.76	1032.8	40	0.022	0.97	0.753	1.30
UTRECH	WDC-CR	52.10	5.12	0	2.76	1032.6	100	0.043	0.78	0.818	1.30
NOVOSI	WDC-CR	54.48	83.00	163	2.87	1012.6	154	0.007	0.99	0.878	1.29
DENVER	WDC-CR	39.67	-104.97	1600	2.91	852.6	31	0.069	0.79	0.739	1.16
HERSTM	WDC-CR	50.87	0.33	23	2.92	1029.9	33	0.043	0.91	0.789	1.32
CLMX	NMDB	39.37	-106.18	3400	3	680.5	299	0.009	0.99	1.002*	1.08
LARC	WDC-CR	-62.20	-58.96	40	3	1026.8	170	0.006	0.99	0.807	1.33
LINDAU	WDC-CR	51.65	10.13	140	3	1015.6	39	0.032	0.95	0.822	1.32
LINIGY	WDC-CR	51.65	10.13	140	3	1015.6	75	0.012	0.98	0.726	1.32
HALLE	WDC-CR	51.48	11.97	100	3.07	1020.5	32	0.065	0.83	0.794	1.33
DRBS	NMDB	50.10	4.60	225	3.18	1005.6	235	0.008	0.97	0.774	1.33
KIEV	WDC-CR	50.43	30.18	120	3.57	1018.2	163	0.008	0.98	0.721	1.41
IRK2	NMDB	52.37	100.55	2000	3.64	810.4	40	0.037	0.94	0.740*	1.25
IRKT	NMDB	52.47	104.03	435	3.64	980.5	66	0.066	0.79	0.801*	1.39
LMKS	NMDB	49.20	20.22	2634	3.84	749.0	71	0.019	0.97	0.882	1.26
MUNCHE	WDC-CR	48.20	11.60	500	4.14	973.3	129	0.007	0.99	0.686	1.47
ZUGSPI	WDC-CR	47.42	10.98	2960	4.24	719.0	243	0.009	0.97	0.745	1.33
DALLAS	WDC-CR	32.98	-96.73	208	4.35	1009.2	102	0.010	0.98	0.681	1.55
HAFELE	WDC-CR	47.31	11.38	2290	4.38	782.2	47	0.016	0.98	0.771	1.39
JUNG	NMDB	46.55	7.98	3570	4.49	665.2	299	0.005	0.99	0.762	1.37
JUNG1	NMDB	46.55	7.98	3475	4.49	673.3	227	0.020	0.87	0.754	1.37
BERKEL	WDC-CR	37.87	-122.27	70	4.54	1025.4	26	0.060	0.81	0.616	1.61
HRMS	NMDB	-34.43	19.23	26	4.58	1031.1	295	0.008	0.96	0.632	1.62
BURE	WDC-CR	44.63	5.91	2252	5	786.1	45	0.051	0.81	0.547*	1.52
PIC_DU	WDC-CR	42.94	0.15	2860	5.36	728.5	146	0.011	0.94	0.561	1.58
USHUAI	WDC-CR	-54.80	-68.32	0	5.68	1032.4	47	0.016	0.96	0.527	1.87
BKSN	NMDB	43.28	42.69	1700	5.7	841.8	97	0.030	0.90	0.687*	1.71
ROME	NMDB	41.00	12.52	60	6.32	1026.3	127	0.012	0.95	0.451*	2.01
AATB	NMDB	43.13	76.55	3340	6.61	685.4	388	0.005	0.96	0.504	1.87
TBILIS	WDC-CR	41.43	44.48	510	6.73	972.8	179	0.009	0.95	0.512	2.05
CALM	NMDB	40.56	-3.16	708	6.95	950.0	35	0.022	0.94	0.378*	2.08
PTFM	NMDB	-26.68	27.09	1351	6.98	880.0	213	0.006	0.96	0.452	2.04
NANM	NMDB	40.37	44.25	2000	7.1	811.5	101	0.034	0.85	0.631*	2.03
BRISBA	WDC-CR	-27.43	153.08	0	7.21	1034.8	27	0.057	0.59	0.303	2.24
TASHKE	WDC-CR	41.20	69.37	565	7.5	966.4	98	0.019	0.90	0.579	2.24
MXCO	NMDB	19.33	-99.18	2274	8.28	786.0	190	0.017	0.72	0.366	2.32
ATHN	NMDB	37.97	23.78	260	8.53	1002.5	48	0.014	0.94	0.364	2.55
TSMB	NMDB	-19.20	17.58	1240	9.15	892.5	345	0.006	0.90	0.364	2.60

Site code	Database name	Lat. (deg)	Lon. (deg)	Elev. (m)	R_c (GV)	x (g cm^{-2})	n (month)	se	R^2	τ	Monitor K
BEIJIN	WDC-CR	39.08	116.26	48	10	1028.0	192	0.017	0.78	0.437	2.98
MORIOK	WDC-CR	39.70	141.13	135	10.16	1017.4	61	0.016	0.91	0.390	3.01
FUKUSH	WDC-CR	37.75	140.48	66	10.46	1025.9	24	0.105	0.65	0.693	3.11
BUENOS	WDC-CR	-34.60	-58.48	0	10.63	1034.2	55	0.015	0.83	0.245	3.17
ESOI	NMDB	33.30	35.80	2055	10.75	806.6	58	0.032	0.67	0.351	2.99
SEOUL	WDC-CR	37.53	126.93	45	10.79	1028.5	39	0.050	0.65	0.418	3.21
SNTIAG	WDC-CR	-33.48	-70.71	570	11	966.5	57	0.007	0.99	0.439	3.18
DJON	NMDB	36.24	127.22	200	11.2	1009.9	97	0.016	0.70	0.186*	3.30
MT_NOR	WDC-CR	36.11	137.55	2770	11.36	737.5	132	0.008	0.95	0.370	3.15
CORDOB	WDC-CR	-31.42	-64.19	434	11.45	982.5	27	0.048	0.46	0.229	3.33
TOKYO	WDC-CR	35.75	139.72	20	11.63	1031.7	169	0.006	0.94	0.317	3.45
MINA_A	WDC-CR	-23.10	-65.70	4000	12.51	631.1	60	0.013	0.94	0.408	3.53
HALESM	WDC-CR	20.72	-156.27	3052	12.91	712.8	178	0.010	0.82	0.275	3.61
HALIGY	WDC-CR	20.72	-156.25	3030	12.91	714.8	166	0.011	0.79	0.266	3.61
HUAN	NMDB	-12.03	-75.33	3400	12.92	682.3	479	0.005	0.89	0.282	3.62
CHACAL	WDC-CR	-16.32	-68.15	5200	13.1	539.2	35	0.022	0.82	0.275	3.80
MAKAPU	WDC-CR	21.30	-157.65	100	13.23	1023.1	65	0.013	0.92	0.366	3.92
KULA	WDC-CR	20.73	-156.33	930	13.3	926.5	52	0.014	0.63	0.134	3.81
TIBET	WDC-CR	30.11	90.53	4300	13.71	606.4	71	0.010	0.94	0.324	3.91
DARWIN	WDC-CR	-12.43	130.87	30	14.09	1032.1	77	0.014	0.70	0.183	4.19
AHMD	NMDB	23.01	72.61	50	15.94	1029.1	66	0.013	0.70	0.157	4.76
PSNM	NMDB	18.59	98.49	2565	16.8	758.0	168	0.009	0.72	0.140*	4.79

435

Appendix B: Derivation of τ from Reference Neutron Monitors

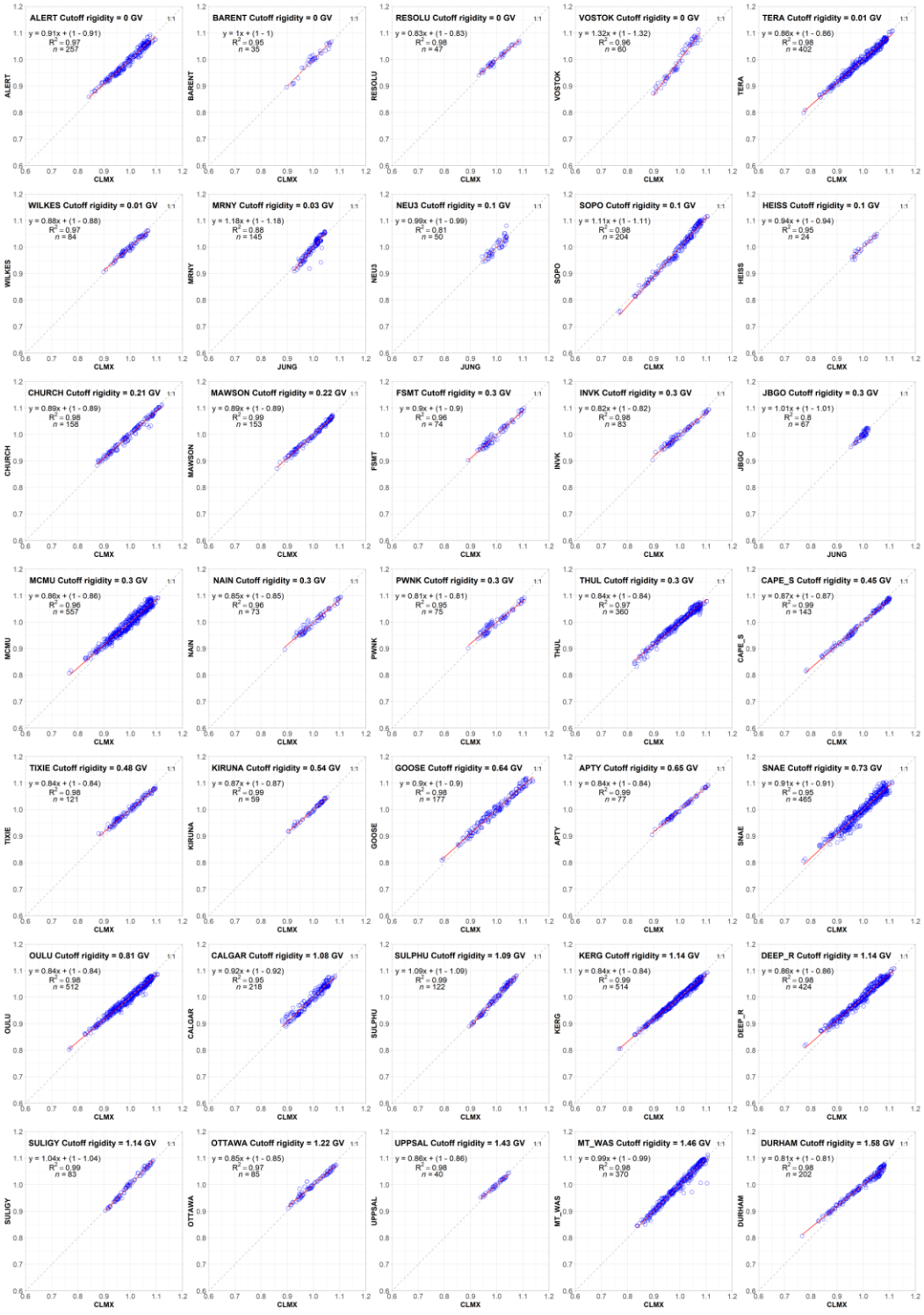

Figure B1. Relationship between normalised reference neutron monitor counts and normalised neutron counts from comparison neutron monitors. Cutoff rigidity or comparison monitors increases from left to right and down the figure.

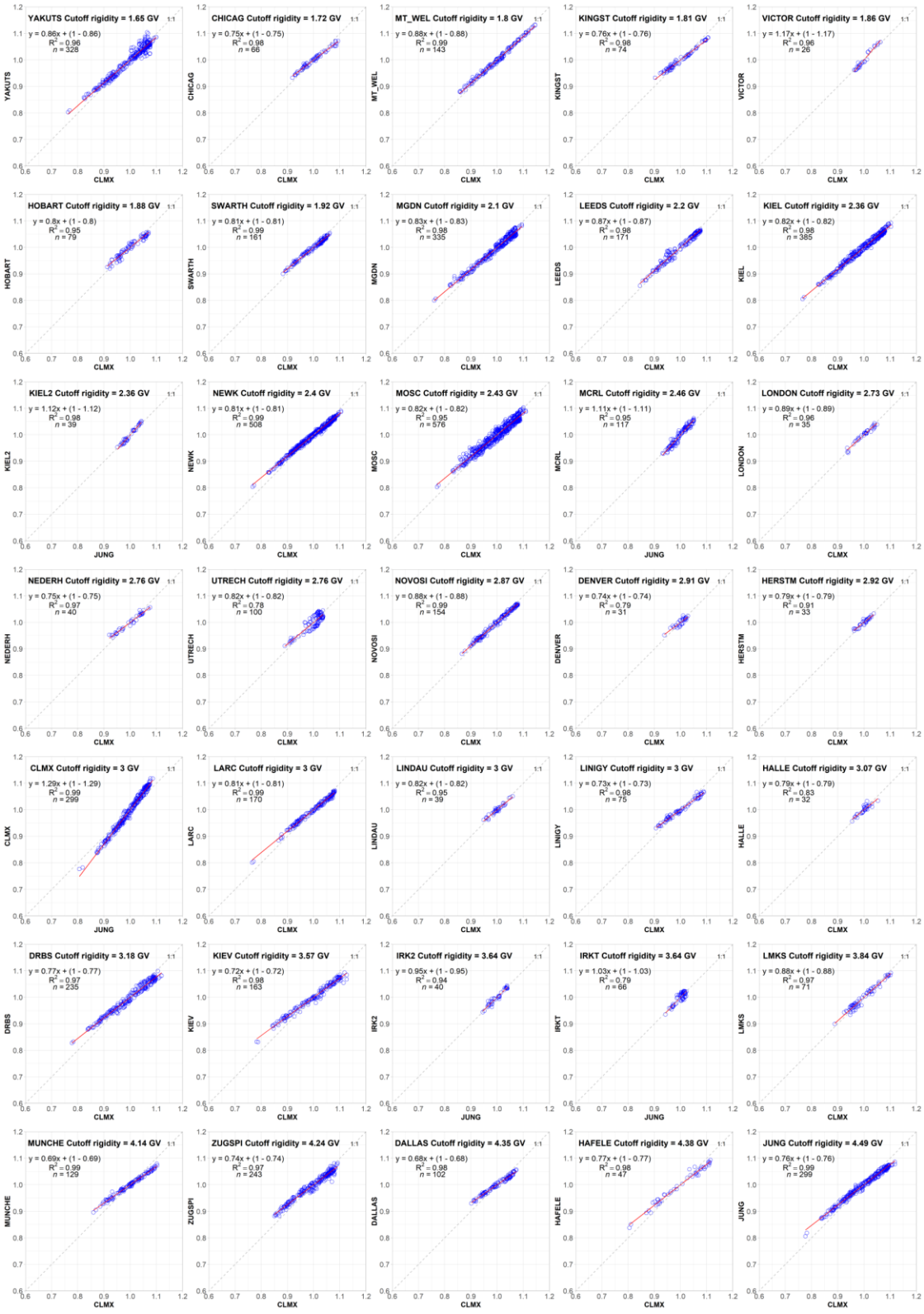

Figure B2. Relationship between normalised reference neutron monitor counts and normalised neutron counts from comparison neutron monitors. Cutoff rigidity or comparison monitors increases from left to right and down the figure.

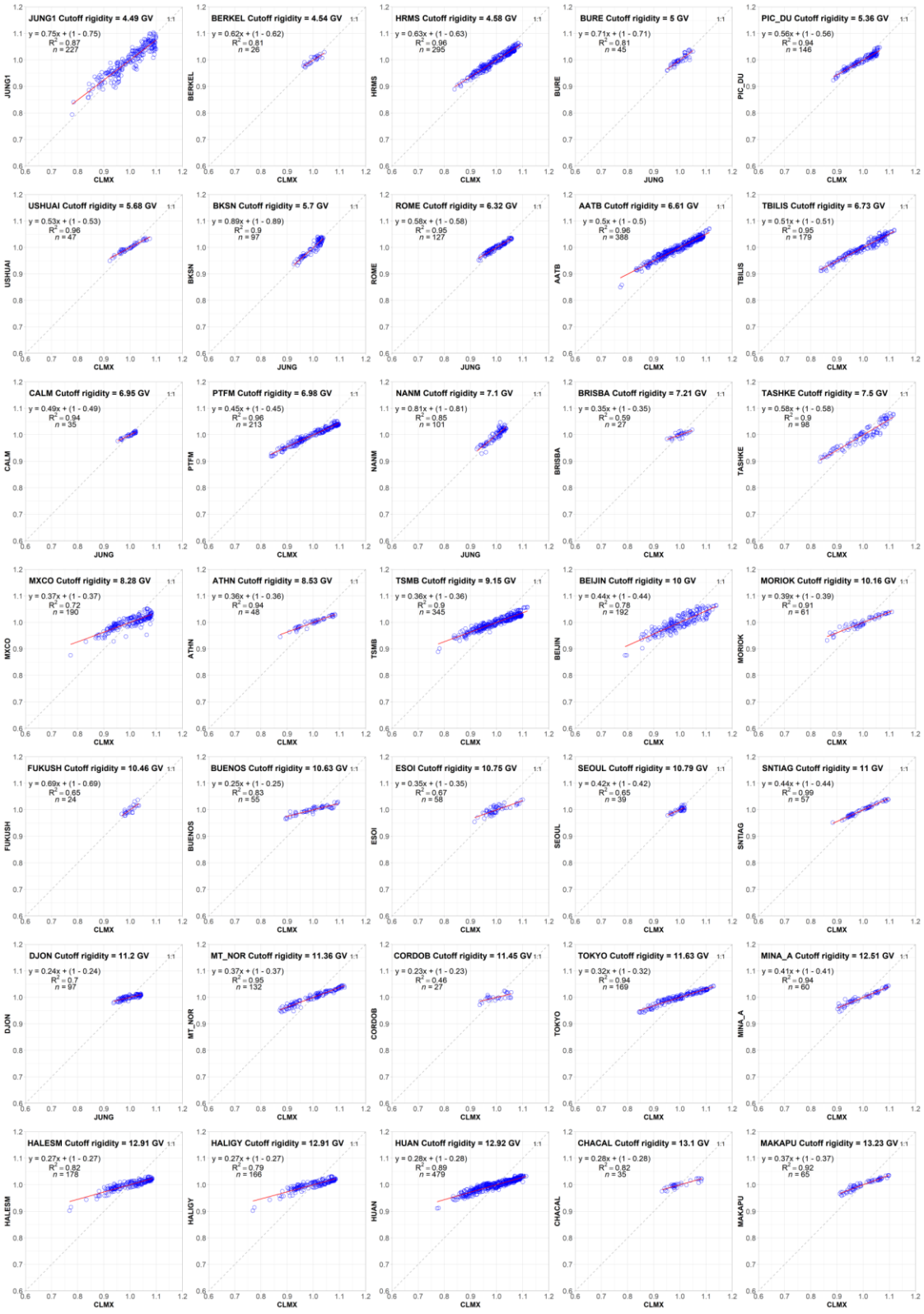

Figure B3. Relationship between normalised reference neutron monitor counts and normalised neutron counts from comparison neutron monitors. Cutoff rigidity or comparison monitors increases from left to right and down the figure.

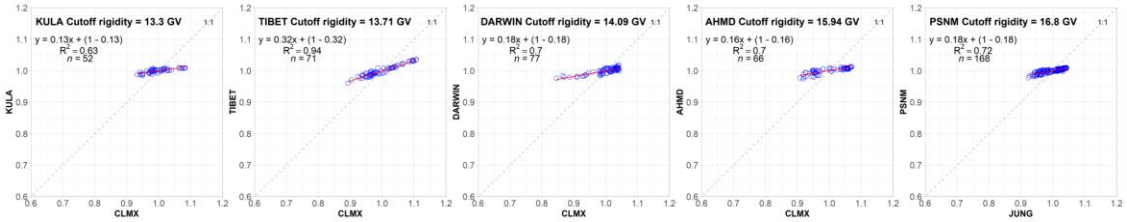

Figure B4. Relationship between normalised reference neutron monitor counts and normalised neutron counts from comparison neutron monitors. Cutoff rigidity or comparison monitors increases from left to right.

References

Baroni, G., Scheiffele, L. M., Schrön, M., Ingwersen, J., & Oswald, S. E. (2018). Uncertainty, sensitivity and improvements in soil moisture estimation with cosmic-ray neutron sensing. *Journal of Hydrology, 564*, 873-887. doi:https://doi.org/10.1016/j.jhydrol.2018.07.053

Bogena, H. R., Huisman, J. A., Baatz, R., Hendricks Franssen, H. J., & Vereecken, H. (2013). Accuracy of the cosmic-ray soil water content probe in humid forest ecosystems: The worst case scenario. *Water Resources Research, 49*(9), 5778-5791. doi:https://doi.org/10.1002/wrcr.20463

Bogena, H. R., Schrön, M., Jakobi, J., Ney, P., Zacharias, S., Andreasen, M., Baatz, R., Boorman, D., Duygu, M. B., Eguibar-Galán, M. A., Fersch, B., Franke, T., Geris, J., González Sanchis, M., Kerr, Y., Korf, T., Mengistu, Z., Mialon, A., Nasta, P., Nitychoruk, J., Pisinaras, V., Rasche, D., Rosolem, R., Said, H., Schattan, P., Zreda, M., Achleitner, S., Albentosa-Hernández, E., Akyürek, Z., Blume, T., del Campo, A., Canone, D., Dimitrova-Petrova, K., Evans, J. G., Ferraris, S., Frances, F., Gisolo, D., Güntner, A., Herrmann, F., Iwema, J., Jensen, K. H., Kunstmann, H., Lidón, A., Looms, M. C., Oswald, S., Panagopoulos, A., Patil, A., Power, D., Rebmann, C., Romano, N., Scheiffele, L., Seneviratne, S., Weltin, G., & Vereecken, H. (2022). COSMOS-Europe: a European network of cosmic-ray neutron soil moisture sensors. *Earth Syst. Sci. Data, 14*(3), 1125-1151. doi:https://doi.org/0.5194/essd-14-1125-2022

Desilets, D., Zreda, M., & Ferre, T. P. A. (2010). Nature's neutron probe: Land surface hydrology at an elusive scale with cosmic rays. *Water Resources Research, 46*. doi:https://doi.org/10.1029/2009wr008726

Dorman, L. I., Fedchenko, S. G., Granitsky, L. V., & Rishe, G. A. (1970). *Coupling and barometer coefficients for measurements of cosmic ray variations at altitudes of 260-400 mb*. Paper presented at the International cosmic ray conference.

Dorman, L. I., Villoresi, G., Iucci, N., Parisi, M., Tyasto, M. I., Danilova, O. A., & Ptitsyna, N. G. (2000). Cosmic ray survey to Antarctica and coupling functions for neutron component near solar minimum (1996– 1997): 3. Geomagnetic effects and coupling functions. *Journal of Geophysical Research: Space Physics, 105*(A9), 21047-21056. doi:https://doi.org/10.1029/2000JA900051

Evans, J. G., Ward, H. C., Blake, J. R., Hewitt, E. J., Morrison, R., Fry, M., Ball, L. A., Doughty, L. C., Libre, J. W., Hitt, O. E., Rylett, D., Ellis, R. J., Warwick, A. C., Brooks, M., Parkes, M. A., Wright, G. M. H., Singer, A. C., Boorman, D. B., & Jenkins, A. (2016). Soil water content in southern England derived from a cosmic-ray soil moisture observing system – COSMOS-UK. *Hydrological Processes, 30*(26), 4987-4999. doi:http://doi.org/10.1002/hyp.10929

Fersch, B., Jagdhuber, T., Schrön, M., Völksch, I., & Jäger, M. (2018). Synergies for Soil Moisture Retrieval Across Scales From Airborne Polarimetric SAR, Cosmic Ray Neutron Roving, and an In Situ Sensor Network. *Water Resources Research, 0*(0). doi:https://doi.org/10.1029/2018WR023337

Flückiger, E. O., & Bütikofer, R. (2009). Swiss neutron monitors and cosmic ray research at Jungfraujoch. *Advances in Space Research, 44*(10), 1155-1159. doi:https://doi.org/10.1016/j.asr.2008.10.043

Franz, T. E., Wang, T., Avery, W., Finkenbiner, C., & Brocca, L. (2015). Combined analysis of soil moisture measurements from roving and fixed cosmic ray neutron probes for multiscale real-time monitoring. *Geophysical Research Letters*, 1-8. doi:https://doi.org/10.1002/2015gl063963

Franz, T. E., Zreda, M., Rosolem, R., & Ferre, T. P. A. (2012). Field Validation of a Cosmic-Ray Neutron Sensor Using a Distributed Sensor Network. *Vadose Zone Journal, 11*(4). doi:https://doi.org/10.2136/vzj2012.0046

Gerontidou, M., Katzourakis, N., Mavromichalaki, H., Yanke, V., & Eroshenko, E. (2021). World grid of cosmic ray vertical cut-off rigidity for the last decade. *Advances in Space Research, 67*(7), 2231-2240. doi:https://doi.org/10.1016/j.asr.2021.01.011

Gleeson, L., & Axford, W. (1968). Solar modulation of galactic cosmic rays. *The Astrophysical Journal, 154*, 1011. doi:https://doi.org/10.1086/149822

Gugerli, R., Desilets, D., & Salzmann, N. (2022). Brief communication: Application of a muonic cosmic ray snow gauge to monitor the snow water equivalent on alpine glaciers. *The Cryosphere, 16*(3), 799-806. doi:https://doi.org/10.5194/tc-16-799-2022

Hawdon, A., McJannet, D., & Wallace, J. (2014). Calibration and correction procedures for cosmic-ray neutron soil moisture probes located across Australia. *Water Resources Research, 50*(6), 5029-5043. doi:https://doi.org/10.1002/2013wr015138

Heber, B., Galsdorf, D., Herbst, K., Gieseler, J., Labrenz, J., Schwerdt, C., Walter, M., Benadé, G., Fuchs, R., Krüger, H., & Moraal, H. (2015). Mini neutron monitor measurements at the Neumayer III station and on

509 the German research vessel Polarstern. *Journal of Physics: Conference Series, 632*, 012057.
510 doi:https://doi.org/10.1088/1742-6596/632/1/012057
511 Howat, I. M., de la Peña, S., Desilets, D., & Womack, G. (2018). Autonomous ice sheet surface mass balance
512 measurements from cosmic rays. *The Cryosphere, 12*(6), 2099-2108. doi:10.5194/tc-12-2099-2018
513 Jitnikovitch, A., Marsh, P., Walker, B., & Desilets, D. (2021). Snow water equivalent measurement in the Arctic
514 based on cosmic ray neutron attenuation. *The Cryosphere, 15*(11), 5227-5239.
515 doi:https://doi.org/10.5194/tc-15-5227-2021
516 Lockwood, M., Stamper, R., & Wild, M. N. (1999). A doubling of the Sun's coronal magnetic field during the past
517 100 years. *Nature, 399*(6735), 437-439. doi:https://doi.org/10.1038/20867
518 Mangeard, P.-S., Ruffolo, D., Sáiz, A., Nuntiyakul, W., Bieber, J. W., Clem, J., Evenson, P., Pyle, R., Duldig, M. L.,
519 & Humble, J. E. (2016). Dependence of the neutron monitor count rate and time delay distribution on the
520 rigidity spectrum of primary cosmic rays. *Journal of Geophysical Research: Space Physics, 121*(12),
521 11,620-611,636. doi:https://doi.org/10.1002/2016JA023515
522 Mavromichalaki, H., Papaioannou, A., Plainaki, C., Sarlanis, C., Souvatzoglou, G., Gerontidou, M., Papailiou, M.,
523 Eroshenko, E., Belov, A., Yanke, V., Flückiger, E. O., Bütikofer, R., Parisi, M., Storini, M., Klein, K. L.,
524 Fuller, N., Steigies, C. T., Rother, O. M., Heber, B., Wimmer-Schweingruber, R. F., Kudela, K., Strharsky,
525 I., Langer, R., Usoskin, I., Ibragimov, A., Chilingaryan, A., Hovsepyan, G., Reymers, A., Yeghikyan, A.,
526 Kryakunova, O., Dryn, E., Nikolayevskiy, N., Dorman, L., & Pustil'nik, L. (2011). Applications and usage
527 of the real-time Neutron Monitor Database. *Advances in Space Research, 47*(12), 2210-2222.
528 doi:https://doi.org/10.1016/j.asr.2010.02.019
529 McJannet, D., Franz, T., Hawdon, A., Boadle, D., Baker, B., Almeida, A., Silberstein, R., Lambert, T., & Desilets,
530 D. (2014). Field testing of the universal calibration function for determination of soil moisture with cosmic-
531 ray neutrons. *Water Resources Research, 50*(6), 5235-5248. doi:https://doi.org/10.1002/2014wr015513
532 McJannet, D., Hawdon, A., Baker, B., Renzullo, L., & Searle, R. (2017). Multiscale soil moisture estimates using
533 static and roving cosmic-ray soil moisture sensors. *Hydrol. Earth Syst. Sci., 21*(12), 6049-6067.
534 doi:https://doi.org/10.5194/hess-21-6049-2017
535 Mishra, S. K., Tiwari, D. P., & Kaushik, S. C. (2005). Study of Forbush decrease event and associated geomagnetic
536 field and cosmic ray intensity varation. *International Journal of Modern Physics A, 20*(29), 6717-6719.
537 doi:https://doi.org/10.1142/s0217751x05029915
538 Rosolem, R., Shuttleworth, W. J., Zreda, M., Franz, T. E., Zeng, X., & Kurc, S. A. (2013). The Effect of
539 Atmospheric Water Vapor on Neutron Count in the Cosmic-Ray Soil Moisture Observing System. *Journal*
540 *of Hydrometeorology*. doi:https://doi.org/10.1175/jhm-d-12-0120.1
541 Schrön, M., Oswald, S. E., Zacharias, S., Kasner, M., Dietrich, P., & Attinger, S. (2021). Neutrons on Rails:
542 Transregional Monitoring of Soil Moisture and Snow Water Equivalent. *Geophysical Research Letters,*
543 *48*(24), e2021GL093924. doi:https://doi.org/10.1029/2021GL093924
544 Schrön, M., Zacharias, S., Köhli, M., Weimar, J., & Dietrich, P. (2015). *Monitoring Environmental Water with*
545 *Ground Albedo Neutrons from Cosmic Rays*. Paper presented at the The 34th International Cosmic Ray
546 Conference, The Hague, The Netherlands.
547 Simpson, J. A. (2000). The Cosmic Ray Nucleonic Component: The Invention and Scientific Uses of the Neutron
548 Monitor – (Keynote Lecture). *Space Science Reviews, 93*(1), 11-32.
549 doi:https://doi.org/10.1023/A:1026567706183
550 U.S. Standard Atmosphere. (1976). US Standard Atmosphere, 1976. *National Oceanic and Atmopsheric*
551 *Administration, 76-1526*.
552 Väisänen, P., Usoskin, I., & Mursula, K. (2021). Seven Decades of Neutron Monitors (1951–2019): Overview and
553 Evaluation of Data Sources. *Journal of Geophysical Research: Space Physics, 126*(5), e2020JA028941.
554 doi:https://doi.org/10.1029/2020JA028941
555 Wallbank, J. R., Cole, S. J., Moore, R. J., Anderson, S. R., & Mellor, E. J. (2021). Estimating snow water equivalent
556 using cosmic-ray neutron sensors from the COSMOS-UK network. *Hydrological Processes, 35*(5), e14048.
557 doi:https://doi.org/10.1002/hyp.14048
558 Zreda, M., Desilets, D., Ferré, T. P. A., & Scott, R. L. (2008). Measuring soil moisture content non-invasively at
559 intermediate spatial scale using cosmic-ray neutrons. *Geophys. Res. Lett., 35*(21), L21402.
560 doi:https://doi.org/10.1029/2008gl035655
561 Zreda, M., Shuttleworth, W. J., Zeng, X., Zweck, C., Desilets, D., Franz, T., & Rosolem, R. (2012). COSMOS: the
562 COsmic-ray Soil Moisture Observing System. *Hydrol. Earth Syst. Sci., 16*(11), 4079-4099.
563 doi:https://doi.org/10.5194/hess-16-4079-2012

564